Evidence of Background-Gradient Effects in GRE-based ^{3}He Diffusion MRI

J. P. Mugler III[1], J. F. Mata[1], T. A. Altes[1,2], G. W. Miller[1], E. E. de Lange[1], W. A. Tobias[1], G. D. Cates Jr. [1], J. R. Brookeman[1]

[1]University of Virginia, Charlottesville, VA, United States, [2]Children's Hospital of Philadelphia, Philadelphia, PA, United States

Introduction: Hyperpolarized ^{3}He diffusion MRI of the human lung permits non-invasive characterization of the pulmonary microstructure [1-3]. For these measurements the apparent diffusion coefficient (ADC) of ^{3}He is determined, typically by using a gradient-echo (GRE) pulse sequence that includes a bipolar gradient waveform for diffusion sensitization. The potential for background gradients (i.e., from any source other than the applied diffusion and imaging gradients) to affect diffusion measurements is well known. Since ^{3}He diffusion MRI commonly uses a GRE-based pulse sequence, and because the lung by nature contains countless air-tissue interfaces, which lead to a very inhomogeneous magnetic environment, it is reasonable to expect that susceptibility-induced background gradients may influence ^{3}He ADC measurements. The purpose of this study was to investigate whether the effects of background gradients could be detected in GRE-based ^{3}He diffusion MRI.

Methods: The measurements were based on a conventional low-flip-angle GRE pulse sequence (TR/TE, 17/12 ms) that used a bipolar gradient waveform for diffusion sensitization [1-3], inserted along the slice-select direction between the excitation RF pulse and signal readout. However, instead of the common single bipolar waveform, two bipolar waveforms were used wherein a time delay could be inserted between the first and second bipolars as illustrated in Fig. 1. For a given measurement, four images were obtained at each slice position during the same acquisition in the standard interleaved fashion used for ^{3}He diffusion MRI. The *b* values for these four images were 0.0, 1.0, 0.0 and 1.0 s/cm^2. For the first *b* value of 1.0 s/cm^2 (2nd image) there was no delay between bipolars, while for the second (4th image) a time delay ranging between 0.8 and 4.8 ms was used. The echo time was identical for all images. ADC maps, and the corresponding means and standard deviations, were calculated from the first and second pairs of images. Pixel-by-pixel ADC ratio images, and the corresponding geometric means and 95% confidence intervals (C.I.), were calculated from the ADC maps.

Under ideal conditions, without background gradients, we expect that the ADC value will be independent of the time delay between the two bipolar waveforms. However, with background gradients, the effective *b* value will depend on the time delay between the bipolars, and increase with the delay. Thus, in the presence of background gradients, the calculated ADC values for the second pair of images should appear higher than those for the first pair because the calculations are based on the ideal *b* value instead of the actual value.

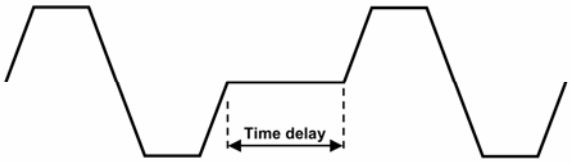

Figure 1. The gradient waveform used for diffusion sensitization, which is composed of two bipolar waveforms separated by a time delay of up to 4.8 ms. The ramp times are 200 μs and the flat-top durations are 400 μs.

Imaging was performed on a 1.5-T scanner (Sonata, Siemens). ^{3}He gas was polarized to ~35% by collisional spin exchange with an optically-pumped rubidium vapor by using a commercial system (Model 9600, MITI). The pulse sequence described above was used to acquire ADC maps from a Tedlar plastic-bag phantom containing 50-ml hyperpolarized ^{3}He and 150-ml N_2 (1 slice covered the whole bag), one New Zealand rabbit (3 coronal slices covered the whole lung), and three human volunteers (1 male, 2 female; age range 19-74; 4-5 25-mm coronal slices spaced evenly across the lung). Two of the human volunteers were healthy; the third had moderate chronic obstructive pulmonary disease (COPD). Prior to imaging, the rabbit was anesthetized with a mixture of Xylazine/Ketamine and intubated with an endotracheal tube. For the gas-bag and human studies, the time delay for the second ADC map was 4.8 ms. For the rabbit study, three acquisitions were performed (during separate breath holds) with time delays of 0.8, 2.4 and 4.8 ms; the most anterior slice was excluded from analysis because the heart occupied roughly 50% of the slice, inducing substantial motion artifacts. Human studies were performed under a Physician's IND (# 57866) for imaging with ^{3}He following a protocol approved by our IRB.

Subject (delay)	ADC_1 [cm^2/s]	ADC_2 [cm^2/s]	ADC change [%]
Gas bag (4.8 ms)	0.914 (0.041)	0.915 (0.041)	0.07 (-0.52, 0.65)
Rabbit (0.8 ms)	0.212 (0.073)	0.221 (0.074)	4.9 (1.6, 8.5)
Rabbit (2.4 ms)	0.210 (0.083)	0.225 (0.080)	9.8 (6.4, 13.2)
Rabbit (4.8 ms)	0.202 (0.076)	0.225 (0.083)	14.1 (9.7, 18.7)
Healthy-1 (4.8 ms)	0.207 (0.051)	0.228 (0.053)	10.5 (9.5, 11.6)
Healthy-2 (4.8 ms)	0.281 (0.058)	0.308 (0.058)	10.4 (9.2, 11.5)
COPD (4.8 ms)	0.584 (0.211)	0.601 (0.202)	4.3 (3.6, 5.0)

Results: The ADC values [mean (S.D.)] from the two maps for each measurement in each subject, and the percent change in the ADC [geometric mean (95% C.I.)] from the ADC ratio images, are presented in the table to the right. The ratios of the mean ADCs were similar to the means of the ADC ratio images. The ADC change for the gas bag was close to zero suggesting, as expected, that there were minimal background gradients. The mean-ADC change for the rabbit increased with time delay, but not linearly as might be expected. (However, a linear increase is within the 95% C.I. for the mean.) Slightly different breath-hold positions for the three acquisitions may have contributed to a deviation from linear behavior and to the lower mean value in the first ADC map for the 4.8-ms delay. The ADC change for the two healthy volunteers was about the same, although the mean ADC values for the second healthy were higher than those for the first. The trachea and main bronchi could be easily visualized in the ADC maps for the second healthy subject. The ADC changes for these regions were close to zero [-0.5% (-1.2, 1.0)], consistent with the hypothesis that background gradients in the lung parenchyma are primarily responsible for the observed changes in ADC values. For the COPD subject the ADC change was lower, and the mean ADC values were higher, than those for the lungs of the healthy subjects. Of greater interest, there were significant regional variations of the ADCs in the COPD subject, and the ADC values demonstrated a strong inverse correlation with the associated ADC ratio values (R^2 = 0.82). This result can be explained as occurring because lung tissue destruction in emphysema should result in a decrease in the surface area of susceptibility interfaces. Note that the inverse relationship between the ADC value and apparent increase in ADC reduces the range of ADC values in the second map because lower ADC values are affected to a greater extent.

Conclusions: For GRE-based ^{3}He diffusion acquisitions that use a pair of bipolar gradient waveforms with an intervening time delay for diffusion sensitization, we observed an increase in the measured ADC with an increase in the time delay and, in a subject with COPD that exhibited a wide range of ADC values within the lung, we observed that this increase is inversely correlated with the ADC value. This result can be explained as arising from the effects of susceptibility-induced background gradients in the lung parenchyma, and suggests that the potential effects of background gradients should be considered when interpreting ADC values, particularly when the diffusion-sensitization period is relatively long or the gradients have relatively small amplitudes. If our results indeed reflect the effects of susceptibility-induced background gradients, then such measurements may provide additional information about the microstructural changes that occur with lung diseases.

References: 1. Saam B, et al. Magn Reson Med 2000;44:174–179. 2. Salerno M, et al. Radiology 2002;222:252-260. 3. Yablonskiy DA, et al. PNAS 2002;99:3111-3116.

Acknowledgements: Supported in part by NIH grant R01-HL079077, CTRF grant IN2002-01 and Siemens Medical Solutions.